Journal of Medicinal Chemistry

Article

pubs.acs.org/jmc

Characterization of 2,4-Diamino-6-oxo-1,6-dihydropyrimidin-5-yl Ureido Based Inhibitors of *Trypanosoma brucei* FolD and Testing for Antiparasitic Activity

Thomas C. Eadsforth,[†] Andrea Pinto,[‡] Rosaria Luciani,[§] Lucia Tamborini,[‡] Gregorio Cullia,[‡] Carlo De Micheli,[‡] Luciana Marinelli,[∥] Sandro Cosconati,[⊥] Ettore Novellino,[∥] Leonardo Lo Presti,[#] Anabela Cordeiro da Silva,[▽] Paola Conti,*[,‡] William N. Hunter,*[,†] and Maria P. Costi*[,§]

[†]Division of Biological Chemistry and Drug Discovery, College of Life Sciences, University of Dundee, Dow Street, Dundee DD1 5EH, U.K.

[‡]Dipartimento di Scienze Farmaceutiche, Università degli Studi di Milano, Via Mangiagalli 25, 20133 Milano, Italy

[§]Department of Life Science, University of Modena and Reggio Emilia, Via Campi 103, 41125, Modena, Italy

[∥]Dipartimento di Farmacia, Università degli Studi di Napoli "Federico II", Via Montesano 49, 80131 Napoli, Italy

[⊥]DiSTABiF, Seconda Università di Napoli, Via Vivaldi 43, 81100 Caserta, Italy

[#]Dipartimento di Chimica, Università degli Studi di Milano, Via Golgi 19, 20133 Milano, Italy

[▽]Instituto de Investigação e Inovação em Saúde, Instituto de Biologia Molecular e Cellular da Universidade do Porto, Departamento de Ciências Biológicas, Universidade do Porto, Porto, Portugal

Supporting Information

ABSTRACT: The bifunctional enzyme N^5,N^{10}-methylenetetrahydrofolate dehydrogenase/cyclo hydrolase (FolD) is essential for growth in Trypanosomatidae. We sought to develop inhibitors of *Trypanosoma brucei* FolD (*Tb*FolD) as potential antiparasitic agents. Compound **2** was synthesized, and the molecular structure was unequivocally assigned through X-ray crystallography of the intermediate compound **3**. Compound **2** showed an IC_{50} of 2.2 μM, against *Tb*FolD and displayed antiparasitic activity against *T. brucei* (IC_{50} 49 μM). Using compound **2**, we were able to obtain the first X-ray structure of *Tb*FolD in the presence of $NADP^+$ and the inhibitor, which then guided the rational design of a new series of potent *Tb*FolD inhibitors.

INTRODUCTION

Kinetoplastidae are flagellated protozoan parasites, including serious human pathogens that are transmitted by different insect vectors. Diseases caused by kinetoplastids include human African trypanosomiasis (HAT, also known as African sleeping sickness), which is due to infection with *Trypanosoma brucei gambiense* or *T. brucei rhodesiense*; Chagas disease, which is caused by *T. cruzi*; and various forms of leishmaniasis caused by infection with different species of *Leishmania*.[1] Those living in tropical and subtropical areas of the world are at risk of contracting these diseases. Sleeping sickness, which is found predominantly across sub-Saharan Africa, is fatal if not treated, and all drugs used in the treatment of HAT have issues relating to efficacy, administration, and side effects. Additionally, increasing levels of drug resistance[2] demonstrate the need for new, improved, and affordable drugs. We have previously identified the bifunctional enzyme FolD as an interesting target for antibacterial drug discovery.[3] This enzyme produces N^{10}-formyl-tetrahydrofolate (THF) in a two-step reaction. First, N^5,N^{10}-methylene-THF is converted to N^5,N^{10}-methenyl-THF by the $NADP^+$ or NAD^+-dependent N^5,N^{10}-methylene-THF dehydrogenase (DH); then, N^{10}-formyl-THF is produced by the action of N^5,N^{10}-methenyl-THF cyclohydrolase (CH, Figure 1).

Received: March 4, 2015
Published: August 31, 2015

DOI: 10.1021/acs.jmedchem.5b00687
J. Med. Chem. 2015, 58, 7938−7948

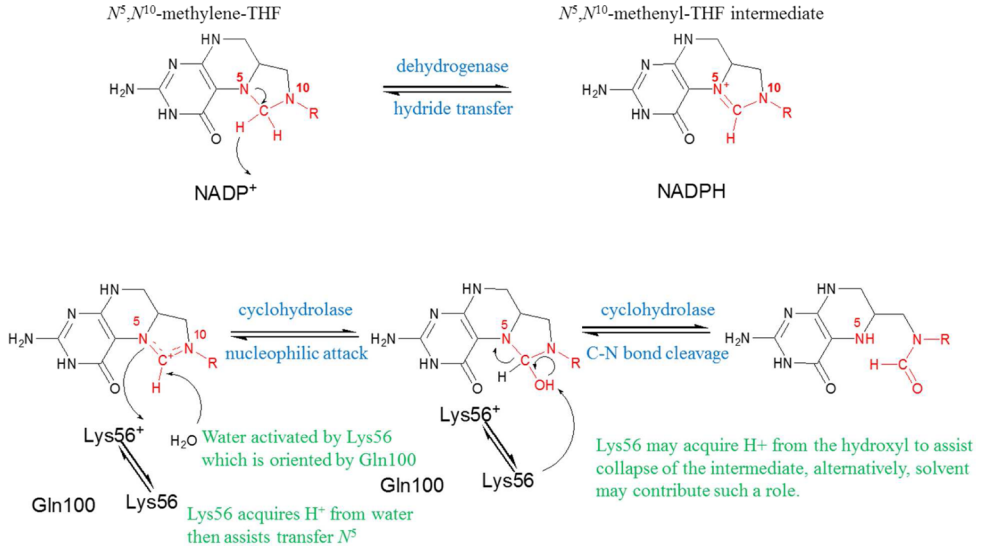

Figure 1. Proposed reaction mechanism of *Tb*FolD.

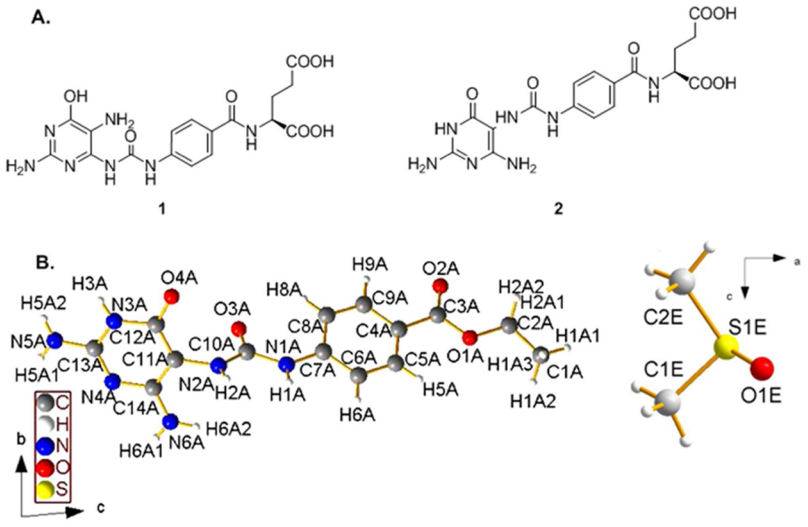

Figure 2. (A) Structures of **1** and **2**; (B) Molecular formula of one symmetry-independent molecule of intermediate **3** and of the DMSO unit showing the atom numbering scheme.

Scheme 1. Synthesis of Compounds 2−5

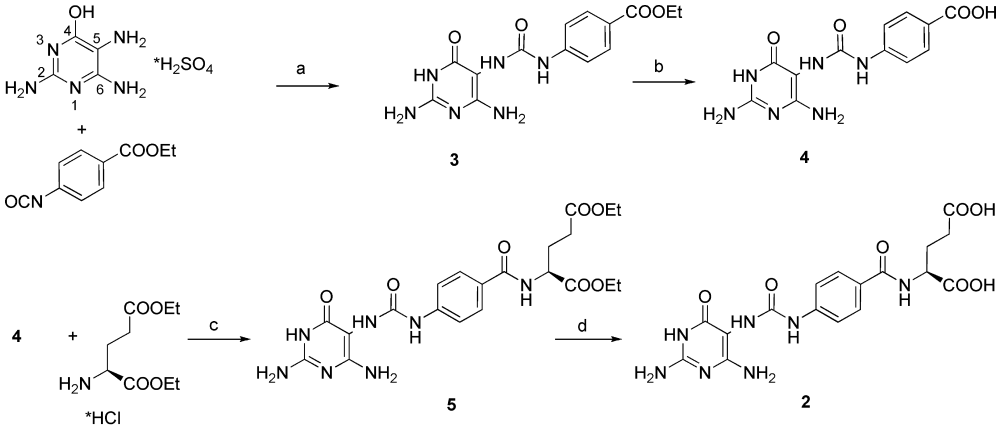

a) 1N NaOH, CH_3CN ; b) 1N NaOH, H_2O; c) *N*-methylmorpholine, 2-chloro-4,6-dimethoxy-1,3,5-triazine, dry DMF; d)1N NaOH

FolD crystal structures have been reported from different organisms,[3−7] including *Leishmania major*[8] but not from *T. brucei*. We initiated an inhibitor discovery program targeting the *T. brucei* enzyme (*Tb*FolD) and selected as a lead compound

DOI: 10.1021/acs.jmedchem.5b00687
J. Med. Chem. 2015, 58, 7938−7948

Scheme 2. Synthesis of Compounds 16−20

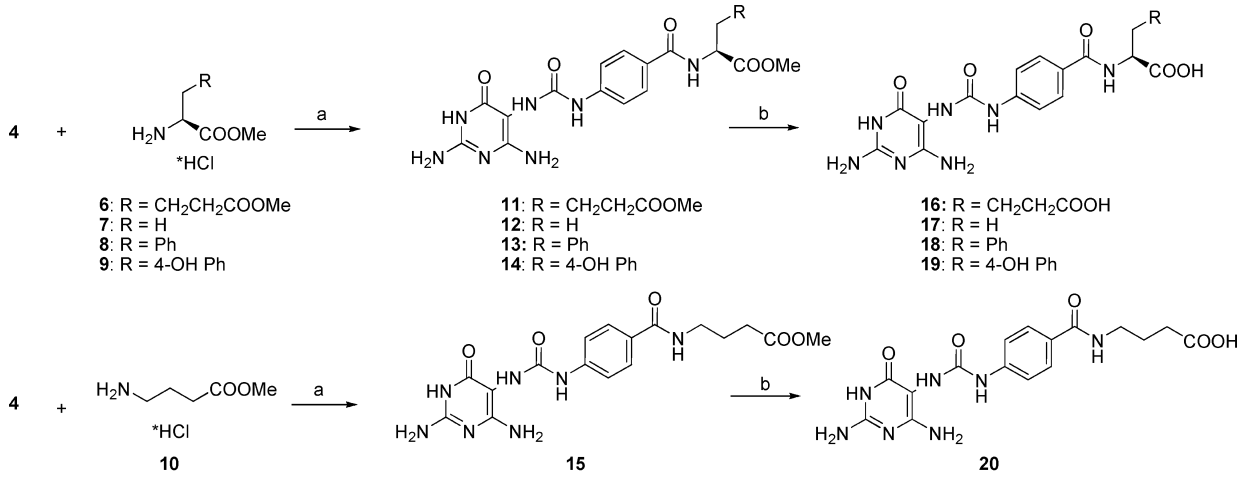

LY374571 (compound **1**) developed by Eli Lilly and Company because it inhibits bacterial and human FolD.[9] However, following the protocol reported for the synthesis of **1**, we obtained a new compound whose structure has been unambiguously determined as **2** (Figure 2). We judge it likely that the original report refers to compound **2** not **1**. To confirm **2** as a suitable lead compound for the development of *Tb*FolD inhibitors, we submitted it to biological evaluation against recombinant *Tb*FolD. Using compound **2**, we were able to obtain the first X-ray structure of *Tb*FolD in the presence of $NADP^+$ and the inhibitor. The X-ray crystal structure of the complex *Tb*FolD-**2**-$NADP^+$ revealed molecular details that were relevant to the binding and inhibition of the enzyme, and allowed, with the help of molecular modeling, a rational design of several analogues (compounds **16−20**). Multiple sequence alignment of FolD from several different organisms (see Figure S1) and superimposition of the corresponding three-dimensional structures provided insight into the major determinants of ligand binding and selectivity for the different FolD forms (see Figure S2). Antiparasitic activity against the bloodstream form of *T. brucei* and cytotoxicity against human leukemia macrophages, differentiated from THP1 monocytes, were evaluated for all compounds under study.

RESULTS

Synthetic Chemistry. Compound **2** was prepared following a procedure[5] originally reported to afford **1** (Figure 2). However, in contrast to what was reported by Schmidt et al.[5] reaction of 4-hydroxy-2,5,6-triaminopyrimidine sulfate with ethyl 4-isocyanatobenzoate (Scheme 1) afforded a derivative with the urea moiety linked at position 5 (compound **3**) instead of position 6. Our structural assignment is based on the X-ray analysis of **3**, which was crystallized as a thin plate by slow evaporation from dimethyl sulfoxide (DMSO). This result provides an important verification of the chemical structure of **2**. Figure 2B shows the molecular formula of one symmetry-independent molecule of **3** with DMSO and the atom numbering scheme (see Supporting Information for details on crystal determination: Figure S3, S4, and S5). CCDC 973826 contains the full supplementary crystallographic data. The latter can be obtained free of charge from the Cambridge Crystallographic Data Centre via www.ccdc.cam.ac.uk/data_request/cif. This structural assignment is in agreement with data reported by Eadsforth et al. dealing with the crystallographic analysis of an *Acinetobacter baumanii* FolD ligand complex.[9]

A series of new analogues of compound **2** were designed on the basis of the crystallographic data and molecular modeling studies, as discussed in detail later. As shown in Scheme 1 intermediate **4** was reacted with a series of different α-amino acids **6−9** or with γ-amino butyric acid **10**, all as methyl esters, using *N*-methylmorpholine and 2-chloro-4,6-dimethoxy-1,3,5-triazine as coupling reagents, affording derivatives **11−15**, which were finally converted into the desired compounds **16−20** by alkaline hydrolysis with 1 N NaOH (Scheme 2).

Single Crystal X-ray Diffraction Analysis of 3. The molecular structure of **3**, as obtained from X-ray diffraction analysis, is shown in Figure S3. The asymmetric unit consists of four independent molecules (labeled A, B, C, and D), each of them being strictly associated with a DMSO host molecule (called E, F, G, and H); see Figure S4. Therefore, the unit cell contains a total of 8 **3**/DMSO adducts. The four unique molecule **3** entities mainly differ by the torsion angles τ between the pyrimidine ring and the ureic moieties (Table S1). In general, the pyrimidine ring is almost perpendicular to the phenyl mean plane, whereas the ureic group roughly lies in the same plane as the phenyl system. For example, the τ(O3-C10-N1-C7) angle is as low as 6(2), 0(2), −2(2) and 7(2) degrees in molecules A, B, C, and D, respectively.

As for the crystal packing, A/B and C/D alternating pairs of closely associated independent molecules are arranged along the [$\bar{1}$10] axis (Figure S5a). Within each pair, a cyclic network of N3−H3···O4 hydrogen-bonded contacts is set up between almost coplanar facing pyrimidine rings (Figure S5b). The other pyrimidinic nitrogen (N4) acts as an acceptor of an intermolecular hydrogen bond donated from the $-N6H_2$ group (Figure S5c), determining the formation of two symmetry-independent infinite hydrogen-bonded *zigzag* ribbons in the (110) plane (Figure S5a). Moreover, the ureic system is involved in hydrogen-bonded contacts with the oxygen of the cocrystallized solvent, whereas the O3 oxygen is a hydrogen-bond acceptor interacting with a neighboring $-N5H_2$ group. Table S2 summarizes all the relevant intermolecular hydrogen-bonded contacts in crystalline **3**.

Crystal Structure of the Ternary *Tb*FolD Inhibitor Complex. The preparation of an efficient recombinant

DOI: 10.1021/acs.jmedchem.5b00687
J. Med. Chem. 2015, 58, 7938−7948

Escherichia coli protein production system as well as the purification, crystallization, and structure determination of *Tb*FolD in a ternary complex with $NADP^+$ and the inhibitor (*S*)-2-(4-(3-(2,4-diamino-6-oxo-1,6-dihydro pyrimidin-5-yl) ureido)benzamido) pentanedioic acid (**2**) is detailed in the Supporting Information. The structure was determined to 2.05 Å resolution. The inhibitor and ADP component of the cofactor were clearly defined by the high-resolution electron density, but the density was less well ordered for the nicotinate moiety.

The *Tb*FolD subunit, which is a polypeptide of 297 amino acids, displays a distinctive tertiary structure typical of this enzyme family. This subunit consists of 11 α-helices and 11 β-strands forming a two-domain structure.[4] *Tb*FolD forms a dimer in solution, as shown by size exclusion chromatography, and a dimer constitutes the asymmetric unit of the crystal structure. Approximately 10% of a subunit surface is occluded from the solvent by dimer formation. The C-terminal domain displays the Rossmann fold and binds $NADP^+$ in a deep cleft. The adenine occupies a hydrophobic pocket near the surface of the enzyme, and the nicotinate is then located between the C- and N-terminal domains. The amino acids that form the cofactor-binding site and interact with the cofactor are highly conserved.[9] We previously noted in different crystal structures of bacterial FolD that the conformation of a loop adjacent to the active site, the β8-α10 loop, was variable. The loop occludes the active site in the structure of the *Pseudomonas aeruginosa* FolD (*Pa*FolD). In the case of the *Tb*FolD, the loop adopts an open configuration, lining and helping to create the active site (Figure S6).

The folate-binding catalytic center is a deep, solvent-filled cavity on the N-terminal domain. Here, **2** binds with an extended conformation (Figure 3). The pyrimidine headgroup

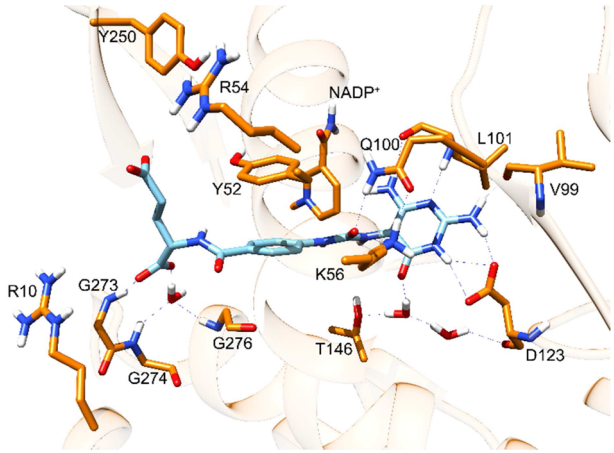

Figure 3. Compound **2** bound in the active site of *Tb*FolD. The polypeptide is depicted as off-white ribbon, the interacting residues, and the nicotinate moiety of the cofactor, which was modeled, are represented with C atoms as orange sticks, the ligand as cyan sticks. All O, N, and H atom positions are red, blue, and white, respectively. Blue dashed lines represent potential hydrogen bonding interactions.

is wedged between K56 and Q100 on one side and I174 (not shown) on the other. The K56 and Q100 side chains are linked together by a hydrogen bond. Direct hydrogen bonding interactions between the inhibitor headgroup and the enzyme involve the side chain of D123, the main chain carbonyls of L101 and V99, and the main chain amide of L101. Additionally, a number of solvent-mediated interactions link **2** O4 to the side chains of K56 and D123. The K56 side chain also binds to the carbonyl group of the linking amide. The **2** benzyl forms π-stacking interactions on one side with Y52; on the other side, there are van der Waals interactions with G276, P277, and T279. The α-carboxylate group of the ligand glutamate moiety participates in a direct charge-reinforced hydrogen bond with the G273 main chain nitrogen and a long-range ionic interaction with the side chain of R10. In similar fashion, the γ-carboxylate interacts with R54. In addition, there are several solvent-mediated interactions that link these acidic groups to G274, G276, and Y250. The side chains of T51, L55, and L252 together with P272 form a hydrophobic clamp to position the tail of the inhibitor.

Molecular Design, Enzyme Inhibition, and SAR Study. Compound **2** was tested for the inhibition of FolD dehydrogenase activity using an established assay.[3] To enlarge the SAR study, we decided to include in the panel of compounds under evaluation also the synthetic intermediates **3**–**5**. The biological data are reported in Table 1. We selected compound LY354899 (**21**), a competitive inhibitor of the human (K_i 29 nM), *Pseudomonas aeruginosa* (30 nM) and *L. major* (105 nM) FolD enzymes,[8,9] as a reference compound, whose structure represents a rigid cyclized analogue of compound **2**. Superimposition of the available *A. baumanii* FolD/**21** structure (PDB code 4V4V) on the *Tb*FolD/**2** complex, herein described, shows that the two ligands adopt the same binding conformation (Figure S7 in Supporting Information). In accordance, compound **21** displayed *Tb*FolD inhibitory activity with a K_i comparable to that of compound **2** (K_i = 8.5 μM and 1.1 μM, respectively).

In stark contrast, the inactivity or very low level of inhibition observed with compounds **3**–**5** confirms that the aforementioned interactions displayed by the glutamate tail are essential for the inhibitory activity. Indeed, both the elimination of the glutamate portion (compounds **3**–**4**) and the esterification of the γ-carboxylate group (compound **5**) led to a significant drop in the inhibitory properties of these compounds.

On the basis of the *Tb*FolD/**2**/$NADP^+$ ternary complex presented here, new compounds **16**–**20** were designed, synthesized, and tested in an enzyme assay. Specifically, compounds **18** and **19** were designed to fill the hydrophobic cleft formed by the side chains of Y52, Y250, L252, and T51. Indeed, derivative **18** (K_i = 0.54 μM) displayed a 2-fold increase of the inhibitory potency, compared to that of compound **2**. In contrast, the lower activity of **19** suggests that the hydroxyl group on the terminal phenyl ring is not well accepted, probably due to its electron-donating properties that unfavorably affect the π–π interaction with Y52 and Y250. We considered that a direct interaction with R54 would be beneficial for inhibition, and compound **16** (K_i = 0.48 μM) was designed for that purpose. The 2-fold increase in the inhibitory potency of this compound, compared to that of compound **2**, seems to confirm our hypothesis.

However, compounds **17** and **20** were synthesized as proof-of-concept for the importance of the Cγ and Cα carboxylate groups, respectively. Both derivatives showed a decreased inhibitory potency, confirming, once again, that at least two strong interactions should be established by the amino acidic tail in order to achieve submicromolar inhibition, either one charge-reinforced H-bond and one ionic interaction, as for compounds **2** and **16**, or one charge-reinforced H-bond and one hydrophobic interaction, as in the case of compound **18**.

DOI: 10.1021/acs.jmedchem.5b00687
J. Med. Chem. 2015, 58, 7938–7948

Table 1. Summary of Compounds' Activity

Code	Compound structure	FolD inhibition[a]	*T. brucei*[b,c]	THP1[b]	SI[d] (THP1/*T. brucei*)
3	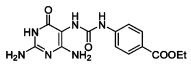	IC_{50}=250±20	89± 2.0	97 ± 4.6	1.1
4	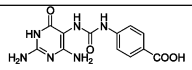	IC_{50}=83 ± 4.3	74 ± 4.0	97 ± 9.6	1.3
5	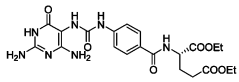	IC_{50}=250±25	92 ± 3.1	205 ± 21	2.2
2	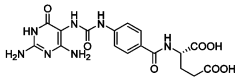	K_i=1.1 ±0.8 IC_{50}=2.2±0.5	49 ± 3.2	194 ± 8.2	4
16	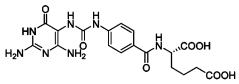	K_i=0.48±0.7 IC_{50}=1.0±0.3	NI	90 ± 16	—
17	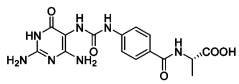	K_i=3.2 ±0.3 IC_{50}=6.3±0.8	NI	113 ± 17	—
18	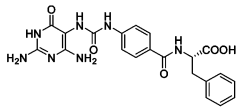	K_i=0.54 ±0.08 IC_{50}=1.1±0.25	NI	94± 8	—
19	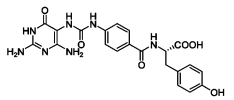	K_i=7.3±0.7 IC_{50}= 9.3±0.9	NI	77± 7	—
20	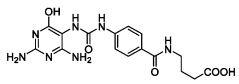	K_i=168±8.5 IC_{50}= 213±18	NI	98± 12	—
21	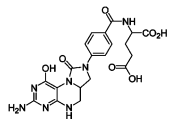	K_i=8.5±0.5 IC_{50}= 20±1.2	57 ± 5.1	103 ± 2.5	1.8

[a] μM. [b] *In vitro* growth inhibition expressed as IC_{50} (μM) of all compounds against the *T. brucei* bloodstream form and human THP1 differentiated macrophages. [c] Pentamidine is the compound of reference (IC_{50} 1.6 ± 0.2 nM). [d] Selectivity index SI = IC_{50}THP/IC_{50} *T. brucei*. NI = no inhibition. Compound structures, enzyme inhibition, antiparasitic activity, and human macrophage growth inhibition are reported.

Molecular Docking. Potential binding poses of **16** and **18**, the most potent inhibitors identified in this series, were calculated by means of Glide 5.5 software in extra precision (XP) mode, using Glidescore for ligand ranking (see below). As shown in Figure 4, the elongation of the γ-carboxylate chain (**16** vs **2**) allows for a salt bridge interaction with the side chains of R54 or R10. Specifically, in the *Tb*FolD-**2**-$NADP^+$ X-ray structure the shortest distance between the **2** carboxylate oxygen and an R54 guanidine hydrogen was around 5 Å, while in the docking-derived pose the same distance is reduced to 2.6 Å. This direct and by implication stronger association is likely the reason for the 2-fold increase in inhibitory potency of **16** with respect to **2**.

Compound **18** was originally designed to fill the hydrophobic pocket shaped by the three residues Y52, Y250, and L252 residues. Indeed, two favored binding poses have been found, one in which the phenyl ring occupies the above-mentioned hydrophobic cleft forming a T-shaping assembly with the two tyrosine residue side chains (see Figure 4) and another in which the ligand phenyl group is directed toward R10 establishing a cation-π interaction (data not shown). However, the lower activity of **19** would perhaps suggest that the latter pose may not be relevant but would support the interaction of the terminal phenyl ring with Y52 and Y25. These latter interactions could be, in turn, the reason for the increased inhibitory potency of **18** with respect to **2**.

Comparison between Human and *T. brucei* FolD Structures. Superimposition of the three-dimensional X-ray structures of human and *Tb*FolDs[5] demonstrates that the enzyme presents a similar structure in these two diverse species

DOI: 10.1021/acs.jmedchem.5b00687
J. Med. Chem. 2015, 58, 7938−7948

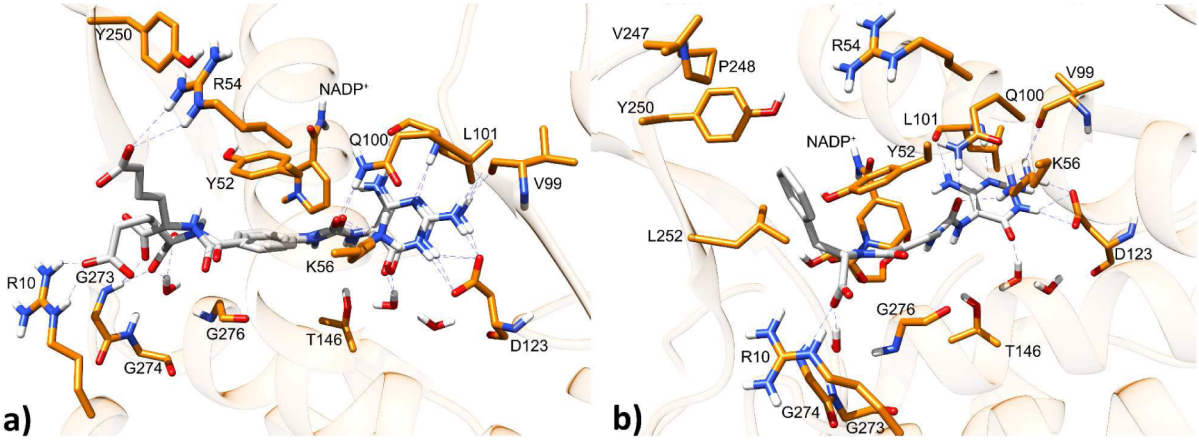

Figure 4. (a) Two possible binding modes of **16** within *Tb*FolD as resulted from docking studies. FolD is shown using the same color scheme employed in Figure 3. The ligand C atoms are represented as white sticks. (b) Binding modes of **18** within *Tb*FolD.

and that the amino acids lining the active sites are overall well conserved (Figure S2, overall sequence identity of 40%). Nevertheless, a number of residues differ between the two enzymes, and a close inspection of the different residues lining the active sites reveals structural differences that could be exploited for the discovery of new trypanocidal agents endowed with low activity against the human FolD. Specifically, in human FolD, residues K10, L51, N54, V55, K175, C236, and I238 are replaced by R10, T51, R54, L55, D173, V236, and T238, respectively, in *Tb*FolD (Figure 5). The lysine–

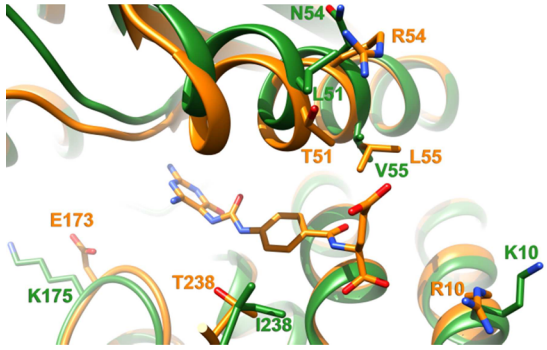

Figure 5. Superimposition of the human FolD (PDB code 1DIG)[5] and *Tb*FolD/**2** (PDB 4LRR) complexes, represented as green and orange ribbons and sticks, respectively. Nonconserved residues between the two species are labeled. The $NADP^+$ cofactor and water molecules were removed for clarity. This picture was obtained using Chimera software (UCSF).[14]

arginine–asparagine–arginine differences at positions 10 and 54 might be targeted to achieve selectivity in inhibitor–enzyme recognition and binding. Both *Tb*FolD R10 and R54 are in close proximity to the glutamate tail of **2** and may be reached via appropriate modification of the ligand's glutamate residue. Thus, the crystal structure of the *Tb*FolD-**2**-$NADP^+$ ternary complex and comparison with the human FolD structure may help address the challenging problem of how to achieve both potency and selectivity toward the parasite and not the human enzyme.

Antiparasitic Activity. All compounds were screened against the bloodstream form of *T. brucei* and showed *in vitro* dose-dependent killing, as determined from the reduction of the resazurin marker for cell viability (Table 1). Despite the fact that several compounds within this series showed a micromolar or even submicromolar activity against the target enzyme *Tb*FolD, they did not display any remarkable antiparasitic activity. Only compounds **2**–**5** showed a moderate antiparasitic activity, and **2** was the most active, with an IC_{50} value of 49 ± 3.2 μM. The reference compound, analogue **21**, exhibited a similar activity. The remaining compounds were inactive. All compounds were less active than suramin, a standard drug used in HAT therapy. A counter-screen testing all compounds with human macrophages differentiated from THP1 monocytes showed more effective toxic activity on the parasite than in mammalian cells. Compounds **2**, **5**, and **21** were 4-, 2.2-, and 1.8-fold more effective, respectively, against the *T. brucei* bloodstream form than against that from human macrophages.

CONCLUSIONS

We have reported the first crystal structure of *Tb*FolD, a potential therapeutic target, with the bonus of obtaining information on the molecular basis of inhibition by compound **2**. This molecule displays a micromolar enzyme inhibitory activity against *Tb*FolD and modest antiparasitic properties. A key part of the analysis was the clear assignment of the molecular structure of **2** using single crystal X-ray analysis of a synthetic intermediate, **3**. The crystal structure of the enzyme–ligand complex provides an accurate template to support structure-based approaches in early stage drug discovery. In addition, we have suggested that, although FolD is a highly conserved enzyme, as indicated by the primary sequence alignment and structural comparisons, some critical differences in the active sites could be exploited to reduce the activity on the human form of the enzyme, and this possibility will be pursued in future development of this class of compounds. Moreover, because molecular recognition is a dynamic process,[10] differences in structural flexibility between the human and *T. brucei* enzymes might provide additional information to support this effort. Despite the fact that almost all compounds showed low micromolar or submicromolar inhibition of *Tb*FolD, the antiparasitic activity on the bloodstream form parasite was modest. Considering the polar nature of these molecules, an explanation for the modest level of antiparasitic activity is that structural modification of the amino acidic tail, while facilitating a better interaction with the target enzyme, has compromised the ability to cross the parasite membrane, likely due to a reduced affinity for membrane

DOI: 10.1021/acs.jmedchem.5b00687
J. Med. Chem. 2015, 58, 7938–7948

transporters. Indeed, very little modification of the Glu chain, such as the one carbon homologation of compound **2** leading to **16**, has produced a complete loss of antiparasitic activity. This suggests that, to obtain more efficacious analogues, also the interaction with membrane transporters should be considered at the onset of the design process.

EXPERIMENTAL SECTION

Material and Methods. All reagents were purchased from Sigma. ^{1}H NMR and ^{13}C NMR spectra were recorded with a Varian Mercury 300 (300 MHz) spectrometer. Chemical shifts (δ) are expressed in ppm, and coupling constants (J) are expressed in Hz. TLC analyses were performed on commercial silica gel 60 F_{254} aluminum sheets; spots were further evidenced by spraying with a dilute alkaline potassium permanganate solution or ninhydrin. Melting points were determined on a model B 540 Büchi apparatus and are uncorrected. Mass spectrometry was carried out on a triple quadrupole spectrometer type Varian 320-MS coupled with ESI source. Elemental analyses were performed on a PerkinElmer PE 2400 elemental analyzer, and the data for C, H, and N were within 0.4% of the theoretical values. All target compounds possessed a purity of ≥95% as verified by elemental analyses by comparison with the theoretical values. (*S*)-2-Aminoadipic acid dimethyl ester hydrochloride **6** was synthesized as previously described.[11]

Synthesis of Ethyl 4-(3-(2,4-diamino-6-oxo-1,6-dihydropyrimidin-5-yl)ureido)benzoate (3). 4-Hydroxy-2,5,6-triaminopyrimidine sulfate (0.91 g, 3.8 mmol) was suspended in water (2 mL) and mixed with a 1 N NaOH solution (11.4 mL). A solution of ethyl 4-isocyanatobenzoate (0.73 mg, 3.8 mmol) in 6 mL of acetonitrile was added dropwise. After stirring at room temperature for 2.5 h, 1 N HCl (11.4 mL) was added, and the mixture was stirred for 5 min. The solid was filtered off and washed with water (50 mL), EtOH (30 mL), and diethyl ether (30 mL). After drying, the product was obtained as a pale orange solid (0.95 g, 2.86 mmol, 75% yield). M.p.: dec >180 °C. ^{1}H NMR (300 MHz, DMSO-d_6) δ (ppm): 10.0 (bs, 1H, -NHCONH-), 8.98 (bs, 1H, -NHCONH−), 7.84 (d, 2H, J = 8.4, Ar−H), 7.57 (d, 2H, J = 8.4, Ar−H), 6.76 (s, 1H, -NH−), 6.16 (bs, 2H, -NH_2), 5.96 (bs, 2H, -NH_2), 4.26 (q, 2H, J = 7.0, CH_2CH_3), 1.31 (t, 3H, J = 7.0, CH_2CH_3). ^{13}C NMR (75 MHz, DMSO-d_6) δ (ppm): 166.22, 162.38, 160.97, 155.26, 154.02, 145.89, 130.89, 122.60, 117.61, 89.94, 60.85, 14.94. MS: 333.0 $[M + H]^+$. Anal. Calcd for $C_{14}H_{16}N_6O_4$: C 50.60, H 4.85, N 25.29; found, C 50.62, H 4.98, N 25.03.

Synthesis of 4-(3-(2,4-Diamino-6-oxo-1,6-dihydropyrimidin-5-yl)ureido)benzoic Acid (4). Compound **3** (0.95 g, 2.86 mmol) was suspended in water (25 mL), and 1 N NaOH (29 mL) was added. The mixture was stirred at room temperature for 3 h, and it slowly turned into a clear solution. 1 N HCl (29 mL) was added, and the precipitate was collected by centrifugation (5000 rpm for 3 min). The solid was sequentially washed and centrifuged (5000 rpm for 3 min) with water (20 mL), EtOH (20 mL), and diethyl ether (20 mL). The product was collected as a pale orange solid (0.80 g, 2.63 mmol, 92% yield). M.p.: dec T > 240 °C. ^{1}H NMR (300 MHz, DMSO-d_6) δ (ppm): 12.50 (bs, 1H, COOH), 9.98 (bs, 1H, -NHCONH-), 8.90 (bs, 1H, -NHCONH−), 7.80 (d, 2H, J = 7.6, Ar−H), 7.52 (d. 2H, J = 7.6, Ar−H), 6.71 (s, 1H, -NH−), 6.18 (bs, 2H, -NH_2), 5.88 (bs, 2H, -NH_2). ^{13}C NMR (75 MHz, DMSO-d_6) δ (ppm): 167.81, 162.20, 160.88, 155.26, 153.98, 145.58, 131.07, 123.50, 117.49, 90.05. MS: 305.0 $[M + H]^+$. Anal. Calcd for $C_{12}H_{12}N_6O_4$: C 47.37, H 3.98, N 27.62; found, C 47.41, H 4.06, N 27.40.

General Procedure for the Synthesis of 5 and Analogues 11−15. A suspension of compound **4** (0.1 g, 0.33 mmol) in dry DMF (7 mL) was placed under a nitrogen atmosphere and sonicated for 5 min. *N*-Methylmorpholine (0.146 mL, 1.32 mmol) was added to the mixture, followed by 2-chloro-4,6-dimethoxy-1,3,5-triazine (232 mg, 1.32 mmol), and the mixture was stirred at 35 °C under nitrogen for 5 h. The suspension slowly turned into an orange-red solution. The desired amino acid (**6−10**) as methyl or ethyl ester hydrochloride (1.32 mmol) was added to the solution followed by *N*-methylmorpholine (0.146 mL, 1.32 mmol), and the mixture was stirred at 30 °C overnight. The solvent was removed under vacuum, keeping the temperature below 45 °C, and the crude mixture was resuspended in EtOH (10 mL) and stirred for 5 min. The solid was recovered by vacuum filtration and washed with EtOH (10 mL) and diethyl ether (10 mL) and finally dried under vacuum overnight.

(*S*)-Diethyl 2-(4-(3-(2,4-diamino-6-oxo-1,6-dihydropyrimidin-5-yl)ureido)benz amido) Pentanedioate (5). Pale orange solid; yield, 70%; m.p., dec T > 180 °C. ^{1}H NMR (300 MHz, DMSO-d_6) δ (ppm): 9.95 (bs, 1H, -NHCONH-), 8.82 (bs, 1H, -NHCONH−), 8.48 (d, 1H, J = 7.0, ArCO-NH-), 7.80 (d, 2H, J = 8.8, Ar−H), 7.50 (d, 2H, J = 8.8, Ar−H), 6.70 (s, 1H, -NH−), 6.18 (bs, 2H, -NH_2), 5.88 (bs, 2H, -NH_2), 4.40−4.37 (m, 1H, Hα), 4.07 (q, 2H, J = 7.3, CH_2CH_3), 4.00 (q, 2H, J = 7.3, CH_2CH_3), 2.45−2.38 (m, 2H, CH_2CH_2COOEt), 2.17−1.95 (m, 2H, $CHCH_2CH_2$COOEt), 1.17 (t, 3H, J = 7.3, CH_2CH_3), 1.13 (t, 3H, J = 7.3, CH_2CH_3). ^{13}C NMR (75 MHz, DMSO-d_6) δ (ppm): 172.92, 172.66, 166.98, 162.17, 160.88, 155.37, 153.95, 144.36, 129.06, 126.59, 117.37, 90.10, 61.17, 60.60, 52.65, 30.91, 26.46, 14.76; MS 490.2 $[M + H]^+$. Anal. Calcd for $C_{21}H_{27}N_7O_7$: C 51.53, H 5.56, N 20.03; found, C 51.61, H 5.60, N 19.91.

(*S*)-Dimethyl 2-(4-(3-(2,4-diamino-6-hydroxypyrimidin-5-yl)-ureido)benzamido)hexanedioate (11). Pale orange solid; yield, 61%; m.p., dec T > 190 °C. ^{1}H NMR (300 MHz, DMSO-d_6) 9.96 (bs, 1H, CONHAr), 8.82 (bs, 1H, Pyrim-NHCO), 8.50 (d, 1H, J = 7.4, CONHCα), 7.77 (d, 2H, J = 8.8, Ar−H), 7.50 (d, 2H, J = 8.8, Ar−H), 6.69 (s, 1H, OH), 6.14 (bs, 2H, -NH_2), 5.88 (bs, 2H, -NH_2), 4.38 (dt, 1H, J = 6.9, 7.4, Hα), 3.62 (s, 3H, OCH_3), 3.56 (s, 3H, OCH_3), 2.32 (t, 2H, J = 7.3, $CH_2CH_2CH_2$COOMe), 1.89−1.72 (m, 2H, $CH_2CH_2CH_2$COOMe), 1.68−1.53 (m, 2H, $CH_2CH_2CH_2COOCH_3$). ^{13}C NMR (75 MHz, DMSO-d_6) 173.76, 173.45, 166.88, 162.29, 160.88, 155.37, 153.97, 144.37, 129.07, 126.53, 117.34, 90.05, 53.00, 52.51, 51.94, 33.46, 30.51, 22.00. MS 476.2 m/z $[M + H]^+$. Anal. Calcd for $C_{20}H_{25}N_7O_7$: C 50.52; H 5.30; N 20.62; found, C 50.62, H 5.58, N 20.43.

(*S*)-Methyl 2-(4-(3-(2,4-diamino-6-hydroxypyrimidin-5-yl)-ureido)benzamido)propanoate (12). Pale orange solid; yield, 69%; m.p., dec T > 182 °C. ^{1}H NMR (300 MHz, DMSO-d_6) 9.98 (bs, 1H, CONHAr), 8.82 (bs, 1H, Pyrim-NHCO), 8.55 (d, 1H, J = 6.9, CONHCα), 7.77 (d, 2H, J = 8.7, Ar−H), 7.50 (d, 2H, J = 8.7, Ar−H), 6.70 (s, 1H, OH), 6.17 (bs, 2H, -NH_2), 5.89 (bs, 2H, -NH_2), 4.43 (dq, 1H, J = 6.9, 7.1, Hα), 3.62 (s, 3H, OCH_3), 1.37 (d, 3H, J = 7.1, $CHCH_3$). ^{13}C NMR (75 MHz, DMSO-d_6) 174.08, 166.52, 162.20, 160.88, 155.37, 153.95, 144.33, 129.03, 126.52, 117.31, 90.03, 52.50, 48.86, 17.49. MS 390.1 m/z $[M + H]^+$. Anal. Calcd for $C_{16}H_{19}N_7O_5$: C 49.35; H 4.92; N 25.18; found, C 49.38, H 4.95, N 24.98.

(*S*)-Methyl 2-(4-(3-(2,4-diamino-6-hydroxypyrimidin-5-yl)-ureido)benzamido)-3-phenylpropanoate (13). Pale orange solid; yield, 58%; m.p., dec T > 170 °C. ^{1}H NMR (300 MHz, DMSO-d_6) 9.98 (bs, 1H, CONHAr), 8.81 (bs, 1H, Pyrim-NHCO), 8.61 (d, 1H, J = 7.0, CONHCα), 7.70 (d, 2H, J = 8.8, Ar−H), 7.48 (d, 2H, J = 8.8, Ar−H), 7.30−7.21 (m, 4H, $CH_2-C_6H_5$), 7.20−7.13 (m, 1H, $CH_2-C_6H_5$), 6.70 (s, 1H, OH), 6.16 (bs, 2H, -NH_2), 5.89 (bs, 2H, -NH_2), 4.60 (ddd, 1H, J = 6.0, 8.0, 9.1, Hα), 3.61 (s, 3H, OCH_3) 3.17−3.04 (m, 2H, J = 7.3, CH_2-C_6H_5). ^{13}C NMR (75 MHz, DMSO-d_6) 173.11, 166.74, 162.27, 160.87, 155.35, 153.96, 144.36, 138.49, 129.74, 128.99, 128.93, 127.15, 126.48, 117.34, 90.05, 54.71, 52.57, 36.97. MS 466.2 m/z $[M + H]^+$. Anal. Calcd for $C_{22}H_{23}N_7O_5$: C 56.77; H 4.98; N 21.06; found, C 56.96, H 5.18, N 20.82.

(*S*)-Methyl 2-(4-(3-(2,4-diamino-6-hydroxypyrimidin-5-yl)-ureido)benzamido)-3-(4-hydroxyphenyl) propanoate (14). Pale orange solid; yield, 59%; m.p., dec T > 175 °C. ^{1}H NMR (300 MHz, DMSO-d_6) 9.97 (bs, 1H, CONHAr), 9.19 (s, 1H, $CH_2-C_6H_4OH$), 8.83 (bs, 1H, Pyrim-NHCO), 8.55 (d, 1H, J = 7.8, CONHCα), 7.70 (d, 2H, J = 8.7, Ar−H), 7.48 (d, 2H, J = 8.7, Ar−H), 7.06 (d, 2H, J = 8.4, $CH_2-C_6H_4OH$), 6.71 (s, 1H, OH), 6.63 (d, 2H, J = 8.4, $CH_2-C_6H_4OH$), 6.15 (bs, 2H, -NH_2), 5.89 (bs, 2H, -NH_2), 4.56−4.45 (m, 1H, Hα), 3.60 (s, 3H, OCH_3), 3.05−2.87 (m, 2H, $CH_2C_6H_4OH$). ^{13}C NMR (75 MHz, DMSO-d_6) 173.26, 166.73, 162.31, 160.89, 156.58, 155.36, 153.97, 144.34, 130.67, 129.00, 128.43, 126.53, 117.30, 115.71, 90.03, 55.37, 52.49, 36.26. MS 482.2 m/z [M +

DOI: 10.1021/acs.jmedchem.5b00687
J. Med. Chem. 2015, 58, 7938−7948

H]$^+$. Anal. Calcd for $C_{22}H_{23}N_7O_6$: C 54.88; H 4.82; N 20.36; found, C, 54.97; H, 4.97; N, 20.01.

Methyl 4-(4-(3-(2,4-diamino-6-hydroxypyrimidin-5-yl)-ureido)benzamido)butanoate (15). Pale orange solid; yield, 63%; m.p., dec T > 210 °C; ^{1}H NMR (300 MHz, DMSO-d_6) 9.98 (bs, 1H, CONHAr), 8.77 (bs, 1H, Pyrim-NHCO), 8.26 (t, 1H, J = 5.5, CONHCH$_2$), 7.71 (d, 2H, J = 8.5, Ar−H), 7.47 (d, 2H, J = 8.5, Ar−H), 6.69 (s, 1H, OH), 6.16 (bs, 2H, -NH$_2$), 5.88 (bs, 2H, -NH$_2$), 3.56 (s, 3H, OCH$_3$), 3.23 (dt, 2H, J = 5.5, 6.6, CH$_2$CH$_2$CH$_2$COOMe), 2.34 (t, 2H, J = 7.1, CH$_2$CH$_2$CH$_2$COOMe), 1.75 (tt, 2H, J = 6.6, 7.1, CH$_2$CH$_2$CH$_2$COOMe). ^{13}C NMR (75 MHz, DMSO-d_6) 173.88, 166.57, 162.28, 160.88, 155.39, 153.96, 143.94, 128.65, 127.49, 117.36, 90.11, 51.92, 39.09, 31.53, 25.28. MS 404.2 m/z [M + H]$^+$. Anal. Calcd for $C_{17}H_{21}N_7O_5$: C 50.62; H 5.25; N 24.31; found, C 50.52, H 5.38, N 24.33.

General Procedure for the Synthesis of 2 and Analogues 16−20. Compound **5** (or analogues **11**−**15**) (0.2 mmol) was dissolved in 1 N NaOH (0.8 mmol), and the solution was stirred at room temperature for 5 h. The solution was neutralized with 1 N HCl, and the precipitate was recovered by vacuum filtration and washed with water (10 mL), EtOH (20 mL), and diethyl ether (20 mL) and finally dried under vacuum overnight.

(*S*)-2-(4-(3-(2,4-Diamino-6-oxo-1,6-dihydropyrimidin-5-yl)-ureido)benzamido)pentanedioic Acid (2). Pale orange solid; yield, 88%; m.p., dec T > 190 °C. ^{1}H NMR (300 MHz, DMSO-d_6) δ (ppm): 12.35 (bs, 1H, COOH), 9.98 (bs, 1H, -NHCONH-), 8.82 (bs, 1H, -NHCONH−), 8.38 (d, 1H, J = 6.6, ArCO-NH-), 7.79 (d, 2H, J = 8.0, Ar−H), 7.50 (d. 2H, J = 8.0, Ar−H), 6.68 (s, 1H, -NH−), 6.18 (bs, 2H, -NH$_2$), 5.90 (bs, 2H, -NH$_2$), 4.40−4.30 (m, 1H, Hα), 2.38−2.30 (m, 2H, CH$_2$CH$_2$COOH), 2.10−2.00 (m, 1H, CHCH$_2$CH$_2$COOH), 2.00−1.90 (m, 1H, CHCH$_2$CH$_2$COOH). ^{13}C NMR (75 MHz, DMSO-d_6) δ (ppm): 174.58, 174.28, 166.85, 162.30, 160.90, 155.39, 153.98, 144.26, 129.01, 126.82, 117.36, 90.10, 52.55, 31.15, 26.68. MS: 434.1 [M + H]$^+$. Anal. Calcd for $C_{17}H_{19}N_7O_7$: C 47.11, H 4.42, N 22.62; found, C 47.20, H 4.50, N 22.46.

(*S*)-2-(4-(3-(2,4-diamino-6-hydroxypyrimidin-5-yl)ureido)-benzamido)hexanedioic Acid (16). Pale orange solid; yield, 78%; m.p., dec T > 205 °C. ^{1}H NMR (300 MHz, d_6-DMSO) 12.26 (bs, 2H, COOH), 9.97 (bs, 1H, CONHAr), 8.80 (bs, 1H, Pyrim-NHCO), 8.35 (d, 1H, J = 7.7, CONHCα), 7.78 (d, 2H, J = 8.7, Ar−H), 7.50 (d, 2H, J = 8.7, Ar−H), 6.69 (s, 1H, OH), 6.14 (bs, 2H, -NH$_2$), 5.87 (bs, 2H, -NH$_2$), 4.31 (dt, 1H, J = 5.1, 7.7, Hα), 2.22 (t, 2H, J = 7.4, CH$_2$CH$_2$CH$_2$COOH), 1.89−1.68 (m, 2H, CH$_2$CH$_2$CH$_2$COOH), 1.68−1.49 (m, 2H, CH$_2$CH$_2$CH$_2$COOCH$_3$). ^{13}C NMR (75 MHz, d_6-DMSO) 174.96, 174.54, 166.69, 162.27, 160.90, 155.38, 153.99, 144.21, 128.97, 126.95, 117.35, 90.14, 53.09, 33.97, 30.90, 22.15. MS 448.1 m/z [M + H]$^+$. Anal. Calcd for $C_{18}H_{21}N_7O_7$: C 48.32; H 4.73; N 21.91; found, C 48.42, H 4.90, N 21.63.

(*S*)-2-(4-(3-(2,4-Diamino-6-hydroxypyrimidin-5-yl)ureido)-benzamido)propanoic Acid (17). Pale orange solid; yield, 70%; m.p., dec T > 195 °C. ^{1}H NMR (300 MHz, DMSO-d_6) 12.44 (bs, 1H, COOH), 9.98 (bs, 1H, CONHAr), 8.82 (bs, 1H, Pyrim-NHCO), 8.40 (d, 1H, J = 7.1, CONHCα), 7.77 (d, 2H, J = 8.8, Ar−H), 7.49 (d, 2H, J = 8.8, Ar−H), 6.69 (s, 1H, OH), 6.13 (bs, 2H, -NH$_2$), 5.87 (bs, 2H, -NH$_2$), 5.74 (s, 1H, OH), 4.37 (dq, 1H, J = 7.1, 7.4, Hα), 1.36 (d, 3H, J = 7.4, CHCH$_3$). ^{13}C NMR (75 MHz, DMSO-d_6) 175.15, 166.33, 162.32, 160.90, 155.40, 153.99, 144.19, 128.94, 126.88, 117.33, 90.07, 48.85, 17.8. MS 376.1 m/z [M + H]$^+$. Anal. Calcd for $C_{15}H_{17}N_7O_5$: C 48.00; H 4.57; N 26.12; found, C 47.84, H 4.78, N 25.93.

(*S*)-2-(4-(3-(2,4-Diamino-6-hydroxypyrimidin-5-yl)ureido)-benzamido)-3-phenylpropanoic Acid (18). Pale orange solid; yield, 72%; m.p., dec T > 180 °C. ^{1}H NMR (300 MHz, DMSO-d_6) 12.76 (bs, 1H, COOH), 9.97 (bs, 1H, CONHAr), 8.79 (bs, 1H, Pyrim-NHCO), 8.46 (d, 1H, J = 8.2, CONHCα), 7.69 (d, 2H, J = 8.8, Ar−H), 7.48 (d, 2H, J = 8.8, Ar−H), 7.33−7.21 (m, 4H, CH$_2$−C$_6$H$_5$), 7.19−7.12 (m, 1H, CH$_2$−C$_6$H$_5$), 6.69 (s, 1H, OH), 6.14 (bs, 2H, -NH$_2$), 5.87 (bs, 2H, -NH$_2$), 4.56 (ddd, 1H, J = 4.6, 8.2, 10.5, Hα), 3.15 (dd, 1H, J = 4.6, 13.8, CH$_2$-C$_6$H$_5$), 3.04 (dd, 1H, J = 10.5, 13.8, CH$_2$-C$_6$H$_5$). ^{13}C NMR (75 MHz, DMSO-d_6) 174.09, 166.64, 162.27, 160.88, 155.35, 153.97, 144.22, 138.99, 129.74, 128.91, 128.85, 126.99, 126.81, 117.33, 90.08, 54.88, 37.01. MS 452.2 m/z [M + H]$^+$. Anal. Calcd for $C_{21}H_{21}N_7O_5$: C 55.87; H 4.69; N 21.72; found, C 55.57, H 4.94, N 21.52.

(*S*)-2-(4-(3-(2,4-Diamino-6-hydroxypyrimidin-5-yl)ureido)-benzamido)-3-(4-hydroxyphenyl)propanoic Acid (19). Pale orange solid; yield: 76%; m.p.: dec T > 198 °C; ^{1}H NMR (300 MHz, DMSO-d_6) 12.61 (bs, 1H, COOH), 9.96 (bs, 1H, CONHAr), 9.16 (s, 1H, CH$_2$−C$_6$H$_4$OH), 8.81 (bs, 1H, Pyrim-NHCO), 8.39 (d, 1H, J = 8.2, CONHCα), 7.69 (d, 2H, J = 8.8, Ar−H), 7.47 (d, 2H, J = 8.8, Ar−H), 7.07 (d, 2H, J = 8.4, CH$_2$−C$_6$H$_4$OH), 6.69 (s, 1H, OH), 6.62 (d, 2H, J = 8.4, CH$_2$−C$_6$H$_4$OH), 6.15 (bs, 2H, -NH$_2$), 5.89 (bs, 2H, -NH$_2$), 4.53−4.41 (m, 1H, Hα), 3.02 (dd, 1H, J = 4.5, 13.8, CH$_2$-C$_6$H$_4$OH), 2.91 (dd, 1H, J = 10.1, 13.8, CH$_2$-C$_6$H$_4$OH); ^{13}C NMR (75 MHz, DMSO-d_6) 174.24, 166.64, 162.27, 160.88, 156.48, 155.37, 153.96, 144.21, 130.66, 128.94, 126.86, 126.81, 117.32, 115.65, 90.03, 55.24, 36.25. MS 468.2 m/z [M + H]$^+$. Anal. Calcd for $C_{21}H_{21}N_7O_6$: C 53.96; H 4.53; N 20.98; found, C 54.12, H 4.78, N 20.64.

4-(4-(3-(2,4-Diamino-6-hydroxypyrimidin-5-yl)ureido)-benzamido)butanoic Acid (20). Pale orange solid; yield, 79%; m.p., dec T > 230 °C. ^{1}H NMR (300 MHz, DMSO-d_6) 12.02 (bs, 1H, COOH), 9.97 (bs, 1H, CONHAr), 8.78 (bs, 1H, Pyrim-NHCO), 8.25 (t, 1H, J = 5.8, CONHCH$_2$), 7.72 (d, 2H, J = 8.8, Ar−H), 7.47 (d, 2H, J = 8.8, Ar−H), 6.68 (s, 1H, OH), 6.13 (bs, 2H, -NH$_2$), 5.86 (bs, 2H, -NH$_2$), 3.23 (dt, 2H, J = 5.8, 6.6, CH$_2$CH$_2$CH$_2$COOH), 2.25 (t, 2H, J = 7.4, CH$_2$CH$_2$CH$_2$COOH), 1.72 (tt, 2H, J = 5.8, 6.6, CH$_2$CH$_2$CH$_2$COOH). ^{13}C NMR (75 MHz, DMSO-d_6) 174.99, 166.56, 162.25, 160.88, 155.39, 153.96, 143.92, 128.64, 127.57, 117.37, 90.16, 39.24, 31.94, 25.36. MS 390.1 m/z [M + H]$^+$. Anal. Calcd for $C_{16}H_{19}N_7O_5$: C 49.35; H 4.92; N 25.18; found, C 49.32, H 4.78, N 25.02.

Molecular Docking. With the aim to test the Glide 5.5 program for its ability to reproduce the crystallized binding geometry of **2**, the latter ligand was subjected to automated docking calculations using extra precision (XP) mode and Glidescore for ligand ranking.[12,13] Before docking, water molecules were removed, while the NADP$^+$ cofactor was retained. The program was successful in reproducing the experimentally found binding mode of **2**, as it corresponds to the best ranked solution with an RMSD of only 0.87 Å. The binding modes of compounds **16** and **18** were accordingly investigated. The herein reported X-ray structure of *Tb*FolD was prepared through the Protein Preparation Wizard within the Maestro 9.0.2112 package using the OPLS-2001 force field. Figures were rendered using the Chimera software package.[14]

Single Crystal X-ray Diffraction Analysis of 3. Compound **3** is poorly soluble in most organic solvents at room temperature, with the exception of DMSO. We therefore tried to grow crystals from DMSO (in different conditions) and from mixtures of DMSO/CH$_3$CN. Eventually, crystallization by slow evaporation (16 days) of a solution of **3** in reagent-grade DMSO (Sigma-Aldrich) at room temperature produced small plates suitable for the determination of the molecular connectivity. After testing several samples, a specimen (0.25 × 0.20 × 0.05 mm^3) grown at the liquor/air interface was selected for the crystallographic analysis. The specimen manifested a significant pleochroism (colorless to violet) under polarized light. It was mounted on the top of a glass capillary fiber in dense perfluorinated oil. The X-ray data collection was performed at room temperature on a 3-circle Bruker SMART APEX goniometer equipped with a CCD APEX-II detector, using graphite-monochromated Mo Kα radiation (λ = 0.71073 Å). A total of 26180 reflections (8144 unique) were recorded up to $(\sin \vartheta/\lambda)_{MAX}$ = 0.5017 Å^{-1}. A high exposure time (120 s/frame) was employed due to the small dimensions of the sample and its very low scattering power. The compound was found to crystallize in the triclinic centrosymmetric P$\bar{1}$ space group (no. 2), with unit cell parameters a = 8.0260(16) Å, b = 10.054(2) Å, c = 48.956(10) Å, α = 84.44(3)°, β = 89.13(3)°, γ = 80.14(3)°, and V = 3873.8(14) Å^3.

Careful visual inspection of the reciprocal lattice showed some weak off-lattice spots attributable to a minor non- merohedral epitaxial twin component of the same **3** phase. Experimental structure factor amplitudes were extracted by integration of the diffraction frames through the SAINT+ program suite,[15] taking into account the

DOI: 10.1021/acs.jmedchem.5b00687
J. Med. Chem. 2015, 58, 7938−7948

presence of the additional lattice. Corrections for sample absorption and X-ray beam anisotropy were applied by the program TWINABS.[16] Eventually, the molecular structure was solved and refined with the SHELX program package.[17] In the final least-squares refined model, the nonmerohedral twinning was explicitly accounted for, and the fractional contribution of the minority component was estimated to be 0.161(3). All of the hydrogen atoms in the asymmetric unit were idealized, and their coordinates were indirectly determined through a "riding motion" constraint. Moreover, all the bonds involving non-H atoms were subjected to a "rigid-bond" restraint, i.e., the component of the atomic anisotropic displacement parameters along the bond direction were restrained to be equal within a tolerance of 0.01 Å^2. This strategy was motivated by (i) the rather poor quality of the sample and, consequently, the relatively low maximum resolution available for the data; (ii) the quite low data-to-parameter ratio (≈ 8), due to the high number of symmetry-unrelated molecules in a large unit cell. However, these drawbacks did not hamper us from reliably determining the molecular connectivity of **3**, even though our estimates for bond distances and angles have, on average, a rather low precision. CCDC 973826 contains the supplementary crystallographic data for this work. The latter can be obtained free of charge from the Cambridge Crystallographic Data Centre via www.ccdc.cam.ac.uk/data_request/cif.

Preparation of a Recombinant Expression System and Purification of *Tb*FolD. The gene encoding 5,10-methylene tetrahydrofolate dehydrogenase/5,10 methenyl tetrahydrofolate cyclohydrolase (*dhch1*) was identified in Genedb (http://www.genedb.org, accession number Tb927.7.1600). Genomic DNA from *T. brucei* (Lister 927 strain) was used as template for PCR with the following primers designed to amplify the *DHCH1* open reading frame using *Nde*I and *Xho1* restriction sites (bold), respectively: 5′-**CAT-ATG**-CCT-GAG-GCG-GTT-G-3′ and 5′-**CTC-GAG**-TCA-CAA-GGC-ACG-AA-3′. The PCR product was inserted into pCR-BluntII-TOPO vector using the Zero Blunt TOPO PCR cloning kit (Invitrogen) prior to excision and ligation into a modified pET15b vector (Novagen) containing a tobacco etch virus (TEV) protease recognition sequence (pET15bTEV). This results in recombinant expression of a product carrying an N-terminal hexa-histidine tag (His-tag), which is cleavable with TEV protease. The recombinant plasmid was amplified in XL-1 blue *E. coli*, and the gene sequence verified by DNA sequencing services (Dundee University), before being transformed into *E. coli* BL21 (DE3) for protein production.

Protein was produced in cells cultured at 37 °C in 1 L LB media containing 50 mg/mL ampicillin. When an OD of 0.8 was attained, expression was induced with IPTG (1 mM) for 16 h at 21 °C. Cells were collected by centrifugation at 4000 rpm for 30 min at 4 °C and frozen at −80 °C until required. After thawing, the cells were resuspended in 50 mM bicine and 50 mM NaCl, pH 8.0 (using 2 mL/g pellet), with the addition of Complete (Roche EDTA-free protease inhibitor) then lysed by sonication (7× 10 s bursts), with cooling to <4 °C between pulses. The lysate was clarified with centrifugation (40000*g*, 30 min, 4 °C). The supernatant was loaded, at 2 mL min^{-1}, onto a HisTrap HP mL column (prepacked with Ni^{2+} Sepharose High Performance-GE Healthcare) equilibrated with buffer 50 mM bicine and 50 mM NaCl, pH 8.0. Unbound protein was removed by washing with 50 mL of this buffer. Retained proteins were eluted with a linear gradient at 1 mL min^{-1} of 0−100% of buffer 50 mM bicine, 50 mM NaCl, and 1 M imidazole, pH 8.0. The sample of *Tb*FolD was passed through a HiTrap Desalting (GE Healthcare) column to exchange the buffer with 50 mM bicine, 250 mM NaCl, 0.5 mM DTT, and 10% glycerol, pH 8.0. The typical yield of protein was approximately 7 mg/L of cell culture. The addition of 10% glycerol in all buffers was required to prevent the loss of activity when the samples were flash-frozen.

Crystallographic Analysis of *Tb*FolD Complexed with Compound 2. Crystallization trials were carried out with a Phoenix Liquid Handling System (Art Robbins Instruments/Rigaku) using commercially available screens (Hampton Research) with a 1:1 ratio of 100 nL of protein solution and an equivalent volume of reservoir equilibrated against a 70 μL reservoir at 20 °C. Crystals, small orthorhombic blocks with approximate dimensions of 0.1 × 0.1 × 0.1 mm^3, were observed after 3 days in conditions with 20% PEG 6000 and 0.1 M citric acid, pH 5.0. We were unable to increase the size of the crystals using hanging drop or sitting drop vapor diffusion methods. Crystals were transferred into a cryo-solution containing the reservoir supplemented with 20% glycerol prior to flash freezing at −173 °C. Crystals were characterized in-house with a Micromax-007 rotating anode generator and R-AXIS IV^{+2} dual image plate detector (Rigaku), prior to storage in liquid nitrogen. X-ray diffraction data were then collected on the microfocus beamline of ID23-2 at the European Synchrotron Radiation Facility (ESRF). Integration and scaling of data were carried out using MOSFLM[18] and SCALA.[19] The crystals belonged to the orthorhombic space group $P2_12_12_1$ with unit cell parameters a = 58.22 Å, b = 77.33 Å, c = 128.91 Å, $\alpha = \beta = \gamma = 90°$. The molecular weight of a subunit is 31.9 kDa, and the asymmetric unit consists of two subunits with a V_M value of 2.79 Å^3 Da^{1-} and solvent content of approximately 55%. Statistics are summarized in Table S3.

The structure of *Tb*FolD was solved by molecular replacement and refined to a resolution of 2.05 Å. The search model was a monomer of the *L. major* FolD structure, which shares a sequence identity of 85% (PDB code A26),[8] with side chains removed. The rotation and translation functions were determined with PHASER[20] with a log likelihood gain of 84. Inspection of the solution in the graphics program COOT[21] showed that a dimer, consistent with gel filtration data, was indeed present. Rigid-body refinement was carried out in REFMAC5.[22] Side chains were built into electron and difference density maps, followed by iterative rounds of restrained refinement, model manipulation, and addition of solvent molecules using COOT and REFMAC5. The final model has R_{work} and R_{free} values of 20% and 24%, respectively. Geometric restrained parameters were manually adjusted and applied in addition to translation/libration/screw analysis (TLS)[23] during the latter stages of refinement. Model quality was checked using MolProbity.[24] Structure superpositions were calculated using LSQKAB,[25] and figures were prepared using PyMOL (Schrödinger LLC).

Enzyme Inhibition Assay. The dehydrogenase activity of FolD was measured spectrophotometrically, using a Beckman DU-640 spectrophotometer, following the formation of 5,10-CH═THF from 5,10-CH_2-THF. 5,10-CH_2-THF dehydrogenase assays were carried out in a 0.5 mL volume at 27 °C and contained 25 mM MOPS, pH 7.3, 30 mM 2-mercaptoethanol, 35 μM mTHF, and 1 mM $NADP^+$. The K_m values of substrate and cofactor having been previously elucidated as approximately 35 and 70 μM. The reaction was initiated by the addition of $NADP^+$ and incubated for 5 min then stopped by the addition of an equal volume of 1 M HCl and the 5,10-CH═THF produced quantified at 350 nm, using an extinction coefficient of 24.9 mM^{-1} cm^{-1}. The enzyme activity was expressed as μ moles 5,10-CH═THF produced per minute. Enzyme inhibition was measured using the dehydrogenase assay, with stocks of compounds dissolved in DMSO (10 mM). The concentration of compound in the first test was 0−50−100 μM. Data from inhibition assays were fitted to a competitive model by linear regression using Origin (OriginLab Corporation).

Cellular Studies. *Trypanosome Culture.* The bloodstream-form *T. brucei brucei* strain 427 was grown in HMI-9 medium −17.66 mg/mL IMDM (Gibco), 3.020 mg/mL sodium bicarbonate (Sigma-Aldrich), 0.136 mg/mL hypoxanthine (Sigma-Aldrich), 0.039 mg/mL thymidine (Sigma-Aldrich), and 0.028 mg/mL bathocuproine sulfonic acid (Sigma-Aldrich) supplemented with 10% heat-inactivated fetal bovine serum (FBS) (BioWhittaker), 1.5 mM L-cysteine hydrochloride monohydrate (Merck), 0.2 mM β-mercaptoethanol (Sigma-Aldrich), 100 U/mL penicillin, and 100 U/mL streptomycin (BioWhittaker) at 37 °C under a humidified 5% CO_2 atmosphere. Cultures were grown in T25 or T75 vented cap culture flasks (Sarstedt) and subcultured every 2−3 days by 100- to 1000-fold dilution, respectively. Parasites were counted directly using a Neubauer chamber (Marienfeld) and diluted appropriately in complete HMI-9 medium.

In Vitro Growth Inhibition Assays. The compounds under study and **21** were tested in a serial drug dilution assay in order to determine

DOI: 10.1021/acs.jmedchem.5b00687
J. Med. Chem. 2015, 58, 7938−7948

the IC_{50} values (concentration of drug causing 50% growth inhibition) by using the Alamar Blue assay.[26] Serial drug dilutions were prepared in 96-well microtiter plates containing culture medium as described above, and wells were inoculated with approximately 2,000 bloodstream form *T. b. brucei* cells. Cultures were incubated for 72 h at 37 °C under a humidified 5% CO_2 atmosphere. After this time, resazurin was added to a concentration of 45.5 μM per well. The plates were incubated for an additional 4 h, and then the fluorescence read in a microplate reader (Sinergy 2, BioTek) using an excitation wavelength of 528 nm and an emission wavelength of 590 nm. The IC_{50} values were calculated by linear regression analysis.

Cytotoxicity. The cytotoxicity of the compounds under study was assessed by a colorimetric MTT assay.[26,27] THP1 differentiated macrophages were seeded at a density of 10^5 cells/well in 96-well plates and allowed to adhere overnight. Cells were incubated with the compound concentration range for 72 h at 37 °C. At the end of the incubation period, 200 μL of 0.5 mg/mL MTT reagent (thiazolyl blue tetrazolium bromide, Sigma) solution was added to each well. The plates were further incubated for 4 h at 37 °C in the dark. The culture medium was subsequently discarded, and 200 μL of isopropanol was added to dissolve the dark-blue formazan crystals. Cell viability was quantified spectrophotometrically by measuring the absorbance of the formazan product at wavelength 570 nm and the background at 660 nm with a microplate reader (Synergy 2, Biotek, USA). The data are expressed as the percentages of viable cells compared to the survival of a control group (untreated cells). The IC_{50} value, i.e., the concentration of compounds necessary to decrease cell viability to 50% of the untreated control was determined by linear regression analysis.

Statistical Analysis. Differences between *in vitro* anti-*Trypanosoma* and THP1 cell cytotoxicity were examined using Student's *t* test. The data are presented as the means ± SD, and all experiments were independently repeated at least three times. *p*-values <0.05 (two-sided) were considered to be statistically significant.

■ ASSOCIATED CONTENT

Supporting Information

The Supporting Information is available free of charge on the ACS Publications website at DOI: 10.1021/acs.jmedchem.5b00687.

SMILES data (CSV)

Details of scaffold identification, library design, X-ray structure analyses, data collection and refinement statistics, experimental methods, and NMR and C, H, and N microanalyses for the synthesized compounds (PDF)

Accession Codes

4LRR

■ AUTHOR INFORMATION

Corresponding Authors

*(P.C.) Phone 0039-02-50319329. Fax: 0039-02-50319326. E-mail: paola.conti@unimi.it.

*(W.N.H.) Phone: 0044-1382-385745. Fax: 0044-1382-385864. E-mail: w.n.hunter@dundee.ac.uk.

*(M.P.C.) Phone: 0039-059-205-5134. Fax: 0039-059-205-5131. E-mail: mariapaola.costi@unimore.it.

Notes

The authors declare no competing financial interest.

■ ACKNOWLEDGMENTS

We acknowledge grants from Ministry of Education and Research (MIUR - project PRIN 2012, grant number 2012-74BNKN), Ministry of Foreign Affairs (Progetto di Grande Rilevanza Italia-Albania, PGR 00102) and Wellcome Trust awards (grant numbers 082596 and 094090, to WNH). We thank the European Synchrotron Radiation facility for the awarded beam time and staff support. We thank Dr. R. Moser of Merck & Cie Schaffhausen (Switzerland) for providing FolD substrate.

■ REFERENCES

(1) Stuart, K.; Brun, R.; Croft, S. Kinetoplastids: related protozoan pathogens, different diseases. *J. Clin. Invest.* **2008**, *118*, 1301−1310.

(2) Wilkinson, S. R.; Kelly, J. M. Trypanocidal drugs: mechanisms, resistance and new targets. *Expert Rev. Mol. Med.* **2009**, *11*, e31.

(3) Eadsforth, T. C.; Gardiner, M.; Maluf, F. V.; McElroy, S.; James, D.; Frearson, J.; Gray, D.; Hunter, W. N. Assessment of *Pseudomonas aeruginosa* N^5,N^{10}-methylenetetrahydrofolate dehydrogenase-cyclo hydrolase as a potential antibacterial drug target. *PLoS One* **2012**, *7*, e35973.

(4) Allaire, M.; Li, Y.; MacKenzie, R. E.; Cygler, M. The 3-D structure of a folate-dependent dehydrogenase/cyclohydrolase bifunctio nal enzyme at 1.5 Å resolution. *Structure* **1998**, *6*, 173−182.

(5) Schmidt, A.; Wu, H.; MacKenzie, R. E.; Chen, V. J.; Bewly, J. R.; Ray, J. E.; Toth, J. E.; Cygler, M. Structures of three inhibitor complexes provide insight into the reaction mechanism of the human methylenetetrahydrofolate dehydrogenase /cyclohydrolase. *Biochemistry* **2000**, *39*, 6325−6335.

(6) Shen, B. W.; Dyer, D. H.; Huang, J. Y.; D'Ari, L.; Rabinowitz, J.; Stoddard, B. L. The crystal structure of a bacterial, bifunctional 5,10 methylene-tetrahydrofolate dehydrogenase/cyclohydrolase. *Protein Sci.* **1999**, *8*, 1342−1349.

(7) Monzingo, A. F.; Breksa, A.; Ernst, S.; Appling, D. R.; Robertus, J. D. The X-ray structure of the NAD-dependent 5,10-methylene tetrahydrofolate dehydrogenase from *Saccharomyces cerevisiae*. *Protein Sci.* **2000**, *9*, 1374−1381.

(8) Eadsforth, T. C.; Cameron, S.; Hunter, W. N. The crystal structure of *Leishmania major* *N*(5),*N*(10)-methylenetetrahydrofolate dehydrogenase/cyclohydrolase and assessment of a potential drug target. *Mol. Biochem. Parasitol.* **2012**, *181*, 178−185.

(9) Eadsforth, T. C.; Maluf, F. V.; Hunter, W. N. *Acinetobacter baumanii* FolD ligand complexes − potent inhibitors of folate metabolism and a re-evaluation of the structure of LY374571. *FEBS J.* **2012**, *279*, 4350−4360.

(10) Ferrari, S.; Costi, P. M.; Wade, R. C. Inhibitor specificity via protein dynamics: insights from the design of antibacterial agents targeted against thymidylate synthase. *Chem. Biol.* **2003**, *10*, 1183−1193.

(11) Kastl, R.; Wennemers, H. Peptide-catalyzed stereoselective conjugate addition reactions generating all-carbon quaternary stereogenic centers. *Angew. Chem., Int. Ed.* **2013**, *52*, 7228−7232.

(12) *Glide*, version 5.5; Schrodinger, LLC: New York, 2009.

(13) *Maestro*, version 9.0.211; Schrodinger, LLC: New York, 2009.

(14) Pettersen, E. F.; Goddard, T. D.; Huang, C. C.; Couch, G. S.; Greenblatt, D. M.; Meng, E. C.; Ferrin, T. E. UCSF Chimera–a visualization system for exploratory research and analysis. *J. Comput. Chem.* **2004**, *25*, 1605−1612.

(15) Bruker. *SMART and SAINT*; Bruker AXS Inc.: Madison, WI, 2005.

(16) Bruker. *SADABS and TWINABS*; Bruker AXS Inc.: Madison, WI, 2007.

(17) Sheldrick, G. M. A short history of SHELX. *Acta Crystallogr., Sect. A: Found. Crystallogr.* **2008**, *A64*, 112−122.

(18) Battye, T. G.; Kontogiannis, L.; Johnson, O.; Powell, H. R.; Leslie, A. G. iMOSFLM: a new graphical interface for diffraction-image processing with MOSFLM. *Acta Crystallogr., Sect. D: Biol. Crystallogr.* **2011**, *D67*, 271−281.

(19) Evans, P. Scaling and assessment of data quality. *Acta Crystallogr., Sect. D: Biol. Crystallogr.* **2006**, *D62*, 72−82.

(20) McCoy, A. J.; Grosse-Kunstleve, R. W.; Adams, P. D.; Winn, M. D.; Storoni, L. C.; Read, R. J. Phaser crystallographic software. *J. Appl. Crystallogr.* **2007**, *40*, 658−674.

DOI: 10.1021/acs.jmedchem.5b00687
J. Med. Chem. 2015, 58, 7938−7948

(21) Emsley, P.; Lohkamp, B.; Scott, W. G.; Cowtan, K. Features and development of Coot. *Acta Crystallogr., Sect. D: Biol. Crystallogr.* **2010**, *D66*, 486−501.
(22) Murshudov, G. N.; Skubák, P.; Lebedev, A. A.; Pannu, N. S.; Steiner, R. A.; Nicholls, R. A.; Winn, M. D.; Long, F.; Vagin, A. A. REFMAC5 for the refinement of macromolecular crystal structures. *Acta Crystallogr., Sect. D: Biol. Crystallogr.* **2011**, *D67*, 355−367.
(23) Painter, J.; Merritt, E. A. Optimal description of a protein structure in terms of multiple groups undergoing TLS motion. *Acta Crystallogr., Sect. D: Biol. Crystallogr.* **2006**, *D62*, 439−450.
(24) Davis, I. W.; Leaver-Fay, A.; Chen, V. B.; Block, J. N.; Kapral, G. J.; Wang, X.; Murray, L. W.; Arendall, W. B.; Snoeyink, J.; Richardson, J. S.; Richardson, D. C. MolProbity: all-atom contacts and structure validation for proteins and nucleic acids. *Nucleic Acids Res.* **2007**, *35*, 375−383.
(25) Kabsch, W. A solution for the best rotation to relate two sets of vectors. *Acta Crystallogr., Sect. A: Cryst. Phys., Diffr., Theor. Gen. Crystallogr.* **1976**, *A32*, 922−923.
(26) Räz, B.; Iten, M.; Grether-Bühler, Y.; Kaminsky, R.; Brun, R. The Alamar Blue assay to determine drug sensitivity of African trypanosomes (T.b. rhodesiense and T.b. gambiense) in vitro. *Acta Trop.* **1997**, *68*, 139−147.
(27) Costa Lima, S. A.; Resende, M.; Silvestre, R.; Tavares, J.; Ouaissi, A.; Lin, P. K.; Cordeiro-da-Silva, A. Characterization and evaluation of BNIPDaoct-loaded PLGA nanoparticles for visceral leishmaniasis: in vitro and in vivo studies. *Nanomedicine* **2012**, *7*, 1839−1849.

DOI: 10.1021/acs.jmedchem.5b00687
J. Med. Chem. 2015, 58, 7938−7948